ACS APPLIED ELECTRONIC MATERIALS

pubs.acs.org/acsaelm Article

X-ray Absorption Fine Structural Study of Atomic Structures and Chemical States of Dopants in 4H-SiC(0001)

Yuhua Tsai, Jingmin Tang, and Yoshiyuki Yamashita*

Cite This: ACS Appl. Electron. Mater. 2023, 5, 3843−3850 Read Online

ACCESS | Metrics & More | Article Recommendations | Supporting Information

ABSTRACT: The atomic structures and chemical states of active and inactive dopant sites in n-type and p-type 4H-SiC(0001) substrates have been investigated by X-ray absorption near edge structure (XANES) and photoelectron spectroscopy (PES). In N atom-doped n-type 4H-SiC(0001), the PES results indicated that a N−C species was formed near the surface. XANES simulations showed that SiNx and N−C species were attributed to active and inactive dopant states, respectively. Angle-resolved XANES measurements showed that the N−C species acted as an inactive dopant site in N-doped 4H-SiC(0001). In Al-doped p-type 4H-SiC, PES analysis revealed that a single chemical state was present at the Al-doped 4H-SiC. The simulated XANES spectra showed that the Si site in 4H-SiC(0001) was replaced by an Al dopant atom, which was the active dopant site. Furthermore, relaxation of the local structure around the Al dopant in Al-doped 4H-SiC(0001) was observed due to bond stretching.

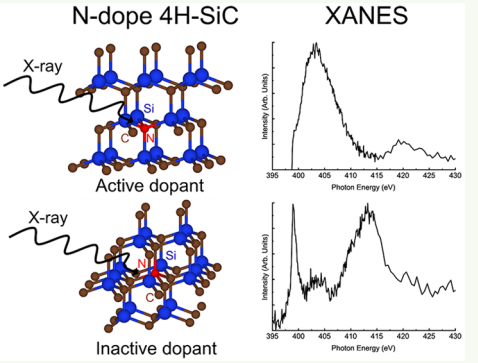

KEYWORDS: *SiC, N-doped SiC, Al-doped SiC, active and inactive dopant*

Downloaded via XIAMEN UNIV on May 23, 2024 at 12:48:36 (UTC).
See https://pubs.acs.org/sharingguidelines for options on how to legitimately share published articles.

1. INTRODUCTION

Silicon carbide (SiC), a wide bandgap semiconductor with an indirect band structure, is attractive as a semiconductor for its excellent physical and electronic properties.[1−3] SiC exhibits a large band gap (2.3 to 3.2 eV), high temperature coefficient, high critical field strength (4−6 MV cm^{-1}), and high chemical stability.[4−6] SiC-based devices show high breakdown voltage, high switching speed, and high-temperature operation.[2,3,7]

SiC has more than 200 polytypes.[3] 3C-SiC can be used for solar cells, piezoresistive devices, and optoelectronic devices.[5] 4H-SiC and 6H-SiC are used in metal-oxide-semiconductor field-effect transistors and high-efficiency photodiodes, respectively. Among the polytypes, 4H-SiC(0001) has received the most attention due to its second-highest bandgap (3.2 eV) and isotropic mobility along the crystal *a*- and *c*-axes.[2] 4H-SiC(0001) is commercially available in a wafer form.[1−3] Nitrogen (N) and phosphorus (P) are used as n-type dopants, whereas aluminum (Al) and boron (B) are used in the case of p-type 4H-SiC.[2,5]

However, using high-concentration doping for n-type or p-type 4H-SiC raises various issues since doping concentration is not equivalent to effective carrier concentration. For N atom-doped n-type 4H-SiC, Ohkubo et al. found that, when the nitrogen concentration reached 10^{19} cm^{-3}, 100% dopant activation could not be obtained.[8] In the previous study by Laube et al., an electrically inactive structure was formed when the N doping concentration reached ∼10^{19} cm^{-3}.[9] For Al atom-doped p-type 4H-SiC, the Al dopants showed fully activated dopants, even though the doping concentration was up to ∼10^{20} cm^{-3}.[10] Furthermore, it has been reported that higher Al doping concentration (∼10^{20} cm^{-3}) resulted in lattice strain.[11]

For SiC, the number of valence electrons is the same at the respective Si and C atoms in SiC. Therefore, it is experimentally unknown whether a dopant atom replaces the Si atom or the C atom in 4H-SiC. In addition, not only the atomic structure and chemical states of active dopant states but also those of inactive dopant states in 4H-SiC have not yet been clarified. Once we clarify the atomic structure and chemical states of the inactive dopant state, we can set a strategy to reduce the inactive dopant concentration.

Various approaches have been attempted to clarify the atomic structures and chemical states of the active and inactive dopant sites in semiconductors. In the case of X-ray diffraction, the atomic structures of dopants cannot be obtained due to the lack of periodicity with such dopants. Atom probe tomography shows the three-dimensional dopant distributions in the film.[12,13] However, chemical information about a dopant cannot be detected. High-resolution scanning transmission electron microscopy can clarify the atomic arrangement of the

Received: April 24, 2023
Accepted: June 8, 2023
Published: June 22, 2023

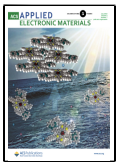

ACS Publications © 2023 American Chemical Society

dopants in real space. However, the detection of elements with a low atomic number is difficult.[14]

In the case of the X-ray absorption near edge structure (XANES), it provides information about the unoccupied states of the corresponding edge element. In addition, using the XANES simulation, we can clarify the atomic structure of the specific atom. Moreover, the extended X-ray absorption fine structure (EXAFS) shows the coordination number of a dopant atom and the interatomic distance between a dopant atom and the nearest neighbor atoms. Thus, we used XANES and EXAFS in this study.

In the present study, we used photoelectron spectroscopy (PES), auger electron spectroscopy (AES), and XANES to elucidate the chemical states and atomic structures of the active and inactive dopant sites in N and Al atom-doped 4H-SiC(0001). Furthermore, EXAFS experiments were employed in Al-doped 4H-SiC(0001) to investigate the interatomic distance between the dopant Al atom and the nearest neighbor atoms.

2. EXPERIMENTAL SECTION

The 4H-SiC(0001) substrates used in this study were purchased from Ceramic Forum Co., Ltd. The epilayers were prepared at Ascatron. The epilayers were grown using a hot-wall chemical vapor deposition system on the 4H-SiC wafers (n^+-type, 4° off-oriented). Using trichlorosilane as the silicon precursor and ethylene as the carbon precursor, 4H-SiC epitaxial layers were prepared. The deposition temperature was set ranging from 1550 to 1650 °C, and the pressure was fixed to 10^4 Pa. For p-type 4H-SiC(0001), Al atoms were used as a dopant. The Al atoms were introduced using trimethylaluminum as the Al source. The concentration was 1×10^{20} cm^{-3}, and the epilayer thickness was 300 nm. In the case of n-type 4H-SiC(0001), N atoms were employed as a dopant. The N atoms were introduced by using nitrogen gas as the N source. The concentration of the dopant was estimated to be 1×10^{19} cm^{-3}, and the epilayer thickness was 5 μm. For electrical activation, thermal annealing at 1450 °C was employed in an argon atmosphere for 30 min. Both doped samples thus prepared were cleaned by standard radio corporation of America so as to remove particles and the surface oxide layer.[15] After the cleaning, contaminated O and C peaks were not detected in the X-ray photoelectron spectroscopy (XPS) spectra (Figures S1 and S2). For the electrodes used in Hall effect measurements, 20 nm-thick Ti was deposited on the 4H-SiC(0001) surface at room temperature (RT) using a sputtering method, and then 150 nm-thick Au was additionally deposited, also at RT, using a sputtering method.

Hall effect measurements showed that the carrier concentration of N-doped 4H-SiC(0001) was estimated to be 5.77×10^{18} cm^{-3} at RT. Thus, inactive dopant sites should exist when the dopant concentration is 10^{19} cm^{-3} because the N dopant was not equal to the carrier concentration. The carrier concentration of Al-doped SiC was estimated to be 1.81×10^{20} cm^{-3} at RT, indicating that Al dopants may be fully activated with a doping concentration of $\sim 10^{20}$ cm^{-3}.

Hard X-ray photoelectron spectroscopy (HAXPES) and X-ray photoelectron spectroscopy (XPS) measurements were performed using a PHI Quantes (ULVAC-PHI). Monochromatic Cr Kα (5414.9 eV) and Al Kα (1486.6 eV) were used as incident X-rays for HAXPES and XPS, respectively. Energy resolutions for HAXPES and XPS were 0.506 and 0.716 eV, respectively. The takeoff angle was set to 90° (surface normal). Survey, O 1s, C 1s, and Si 2p XPS spectra for N- and Al-doped 4H-SiC are shown in Figures S1 and S2.

PES, Auger electron spectroscopy (AES), XANES, and EXAFS measurements were conducted at the BL1N2 and BL7U beamlines in the Aichi Synchrotron Radiation Center. The XANES and EXAFS measurements were carried out at BL1N2 for Al-doped 4H-SiC(0001). In the BL1N2 beamline, the base pressure of the main chamber (the measurement room) was 1.0×10^{-6} Pa. We used a SCIENTA R3000 as an electron analyzer. The angle between the incident X-ray photon and the electron analyzer was 45°. The takeoff angle was set to 90° (surface normal).[16] For the EXAFS measurements, the total electron yield (TEY) was employed. The energy range for the EXAFS measurements was 1500 to 1806 eV. For N-doped 4H-SiC(0001), we performed PES, AES, and XANES measurements at BL7U. In the BL7U beamline, the base pressure of the main chamber was approximately 1.5×10^{-8} Pa. The spot-size of the beam at the sample position was ~0.05 × ~0.07 mm (horizontal × vertical). We used MBS A-1, MB Scientific AB, as the electron analyzer. The energy resolution was 40 meV of the PES spectra. The angle between the incident X-ray and the electron analyzer was 45°. The takeoff angle was set to 90° (surface normal) for PES and AES measurements. A Au film was used for the energy calibration in both beamlines.

For the XANES simulations, we used FEFF9.[8,17−22] We employed full multiple scattering, self-consistent field, Hedin-Lundqvist (HL) exchange-correlation potential, and the final-state effect (Z+1 approximation).[17,23,24]

3. RESULTS AND DISCUSSION

3.1. N-Doped 4H-SiC(0001). Figure 1 shows the Si 1s core-level HAXPES spectrum for N-doped 4H-SiC(0001).

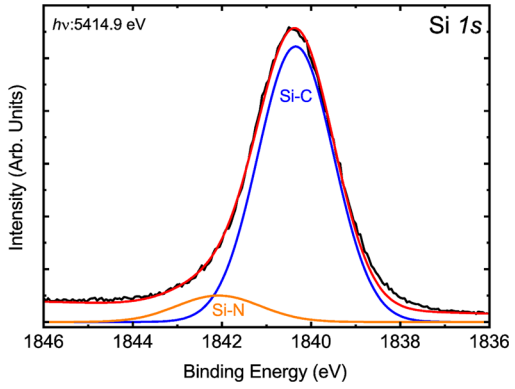

Figure 1. Si 1s core-level HAXPES spectrum for N-doped 4H-SiC(0001) measured at a photon energy of 5414.9 eV.

The peak at 1840.4 eV is attributed to the Si−C species, while the peak at 1842.1 eV is due to the Si−N species.[17,25,26]

Figure 2 shows N 1s core-level spectra measured with photon energies of 520 and 1486.6 eV for N-doped 4H-SiC(0001). The peak at 397.2 eV is attributed to the N−Si species (SiNx),[27,28] whereas the peak at 398.6 eV is assigned to the N−C species.[29−33]

As can be seen, the areal intensities of the SiNx and N−C species depend on the incident photon energies. In the case of a photon energy of 1486.6 eV (Al Kα, XPS), the areal intensity ratio (I_{NC}/I_{SiNx}) is 0.153. For a photon energy of 520 eV, this intensity ratio increases to 0.513. In the case of photon energy of 1486.6 eV, photoelectron kinetic energy is ~1085 eV at the N 1s core level, while the kinetic energy is ~120 eV in the case of photon energy of 520 eV. Because lower kinetic energy indicates more surface sensitivity,[17,34] the N−C species is predominantly formed near the surface. Note that the areal intensity ratio (I_{SiN}/I_{SiC}) in the Si 2p spectrum (Figure S1) is 0.148, whereas the areal intensity ratio in the Si 1s spectrum (Figure 1) is 0.106. Because the emitted photoelectrons in Si 1s core level exhibit lower kinetic energy than those in Si 2p core level, the Si−N species is predominantly formed near the surface. Thus, the order of surface sensitivity is the N−C species, the N−Si species, and the Si−C species.

https://doi.org/10.1021/acsaelm.3c00546
ACS Appl. Electron. Mater. 2023, 5, 3843−3850

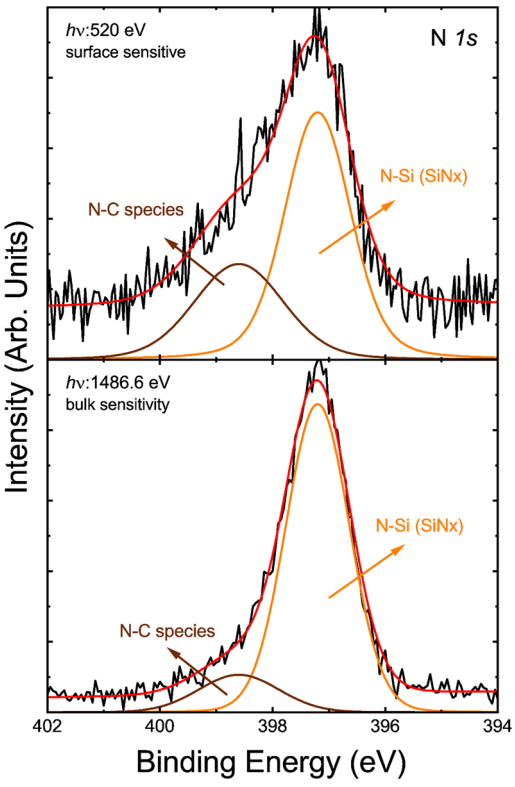

Figure 2. N 1s core-level spectra measured at photon energies of 1486.6 and 520 eV for N-doped 4H-SiC(0001). In the case of a photon energy of 1486.6 eV, the standard XPS measurements was employed. In the case of a photon energy of 520 eV, BL7U was used to obtain the spectrum.

In order to perform chemical state discriminated XANES using Auger electron yield (AEY), we measured the AES spectrum. Figure 3 shows the N−KVV AES spectrum for N-doped 4H-SiC(0001) measured at an incident photon energy of 430 eV. Note that because the Auger electron emitted processes are very complicated, it is very difficult to perform peak fitting. Here, we assumed that the peak fitting can be employed by the Voigt function in the AES spectrum. Since there are two chemical species in the PES spectrum (Figure 2), our AES spectrum should show two chemical species. In addition, the N−KVV AES appears too wide compared to the standard N−KVV AES.[35,36] Therefore, two chemical species should be present in the N−KVV AES; the peaks at lower and higher kinetic energies (KEs) may be 374.2 and 378.9 eV, respectively. According to the previous study by J. M. Ripalda et al., the C−N bonds show the peak at 382 eV in N−KVV AES spectrum.[37] On the other hand, H. H. Madden et al. reported that the Si−N component is observed at ∼379 eV in the N−KVV AES spectrum.[38] The peak energy difference of ∼3 eV between the C−N and Si−N species is in good agreement with our result in the N−KVV AES spectrum. In addition, for n-type semiconductors, the Fermi level is located at the conduction band minimum, shifting to a lower KE direction. Therefore, the lower KE component at 374.2 eV may be attributed to N−Si species, whereas the higher KE component at 378.9 eV might be due to the N−C species. Note that the information depth of KE of 376 eV is estimated to be 3.3 nm.[39,40] Therefore, the AES spectra show near surface information.

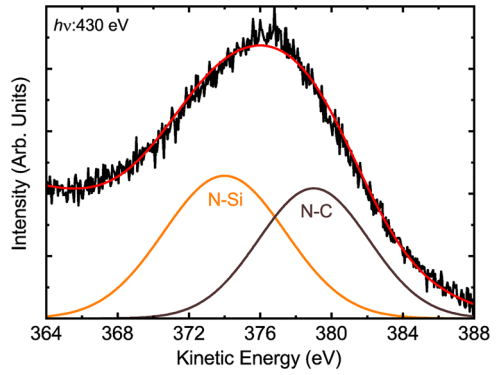

Figure 3. N−KVV AES spectrum for N-doped SiC measured at a photon energy of 430 eV.

Figure 4 shows the N K-edge experimental XANES spectra and simulated XANES spectra for N-doped 4H-SiC(0001). The N K-edge XANES spectrum (Figure 4(a)) is measured with the Auger electron yield (AEY) of the N−Si species (KE of 370 eV). Three pronounced components can be observed at 399.2, 403.5, and 420.0 eV in the spectrum. The N−K-edge XANES spectrum (Figure 4(b)) is measured with the AEY of the N−C component (KE of 382 eV). In the spectrum, there are three main features at 399.0, 403.6, and 413.7 eV. Note that we did not select the peak tops of N−Si and N−C species in Figure 3 for the XANES measurements. This is because a contribution from the overlap of another peak is prevented.

For N−C species, the main peak at 399.0 eV is attributed to the transition of the N 1s→ π^* state of carbon nitride structures.[41−43] The peak at 403.6 eV is from the sp^2-hybridized nitrogenated carbon reported by Jiménez et al.[44] According to a previous study, these two orbital peaks at 400.0 and 403.7 eV have e_{2u} symmetry and b_{2g} symmetry, respectively.[45] Therefore, we can assign the peak at 399.0 eV to 1s→ π^*state transitions with e_{2u} symmetry, while the peak at 403.6 eV is assigned to 1s→ π^* state transitions with b_{2g} symmetry.[42,43,46,47] The peak at 413.7 eV is attributed to the 1s→ σ^* state transition.[42,48−50]

In order to clarify the atomic structures of the two kinds of dopant states for N-doped 4H-SiC(0001), we employed XANES simulations. For the simulations, a cluster size of ∼350 atoms (0.95 nm radius) was employed. In the 4H-SiC, all atoms in the matrix have the same valence, so the nitrogen dopant incorporation site does not affect the doping type.[51] Figures 4(c) and 4(d) show the local atomic structure and the XANES simulation for the C substitutional (N_C) site. Figures 4(e) and 4(f) show the local atomic structure and the XANES simulation for the Si substitutional (N_{Si}) site. For the simulated XANES spectrum for N_C (Figure 4(d)), three main peaks are observed at 401.5, 405.4, and 420.0 eV, which is very similar to the experimental results for XANES of an N−Si structure (Figure 4(a)). For the simulated results, the main peak at 405.4 eV is related to π^* state transitions of Si−N bond, while the peak at 420 eV is attributed to the σ^* state transitions.[52] This result is in good agreement with a previous study focused on N_C sites in SiC.[8,25,52] Accordingly, we conclude that SiNx is attributed to N_C.

In order to represent the experimental XANES of N−C species, we have changed the bond length of the N−C species. We found that N−C bond length of 1.5 Å represented the experimental XANES of N−C species (see Figure S3). Figure 4(f) shows the simulated XANES spectrum for N_{Si}. In the

https://doi.org/10.1021/acsaelm.3c00546
ACS Appl. Electron. Mater. 2023, 5, 3843−3850

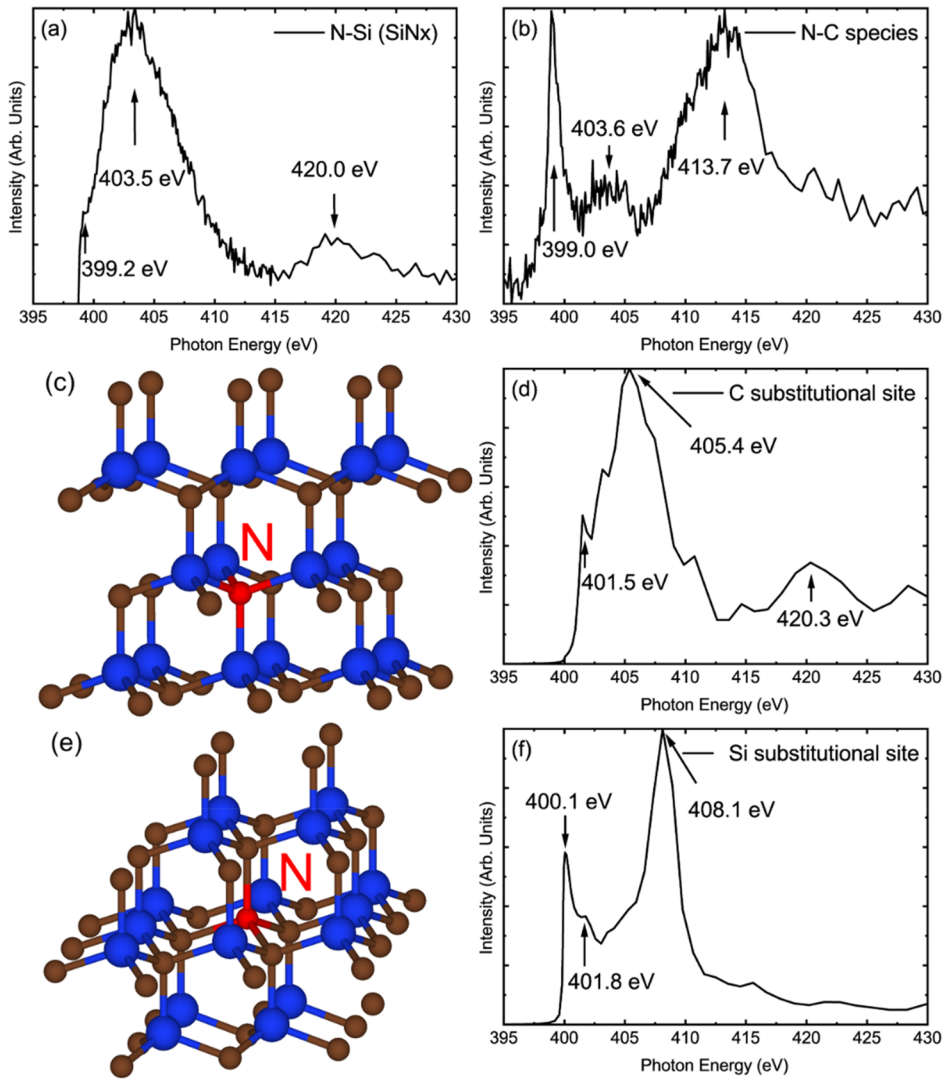

Figure 4. N K-edge XANES spectra measured at AEY and the simulated XANES spectra. (a) Experimental AEY of 370 eV. (b) the experimental AEY of 382 eV. The takeoff angle was set to 90° (surface normal) for (a) and (b). (c) Local atomic structure of N atom in 4H-SiC for the N_C site. (d) Simulated XANES spectrum for the N_C site. (e) Local atomic structure of N atom in 4H-SiC for the N_{Si} site where the N−C bond length is 1.5 Å. (f) Simulated XANES spectrum for N_{Si} site. Dark blue, brown, and red circles in parts (c) and (e) indicate Si, C, and N atoms, respectively.

simulated spectrum, three peaks at 400.1, 401.8, and 408.1 eV are observed. The peaks at 400.1 and 401.8 eV are attributed to 1s→ 2p splitting π^* state transition from the N−C bond, whereas the peak at 408.1 eV is due to the 1s→ σ^* in N−C bonds.[42,43] The simulation spectrum is in fair agreement with the experimental XANES of the N−C species. Therefore, the N−C species is due to N_{Si}. Note that the interstitial sites and the vacancies did not represent experimental results (see Figure S4).

Figures 5(a) and 5(b) show angle-dependent XANES spectra of SiNx and N−C species, respectively. In Figure 5(a), the XANES spectra of SiNx do not depend on the takeoff angle, indicating that the SiNx structure is uniformly formed in the N-doped 4H-SiC(0001). For the N−C species (Figure 4(b)), on the other hand, the intensity changes significantly depending on the takeoff angle.

Since the dopant is introduced uniformly, the SiNx structure shows homogeneous formation in N-doped 4H-SiC(0001); that is, N_C is attributed to an active dopant structure. According to the previous studies based on density functional theory (DFT) calculation, the formation energy of N_C is much lower than that of N_{Si}, which is in good agreement with our results.[51,53] The N−C species (N_{Si}), on the other hand, acts as the electrically inactive structure, because it is predominantly formed near the surface.

3.2. Al-Doped 4H-SiC(0001). Figure 6 shows the XPS spectrum for Al-doped 4H-SiC(0001). In the spectrum, only one peak is observed at 71.2 eV, implying that the dopant Al atom exhibits a single chemical state. Note that the binding energy of dopant Al atoms shows a lower binding energy than metal Al. This is because, for p-type semiconductors, the Fermi level is located just above the valence band maximum. For nondoped semiconductors, Fermi level may be located at midgap. The Fermi level energy difference is about half of the band gap energy, shifting the lower binding energy of a dopant in the case of p-type dopants. For wide-bandgap semiconductors, the energy shift is large. Thus, the Al dopant shows a lower binding energy than metal Al. This phenomenon is observed in p-type wide-bandgap semiconductors.[54]

Figure 7(a) shows the Al K-edge XANES spectrum for Al-doped 4H-SiC(0001) measured by TEY and the simulated XANES spectra. In the experiment's XANES spectrum, a pre-

https://doi.org/10.1021/acsaelm.3c00546
ACS Appl. Electron. Mater. 2023, 5, 3843−3850

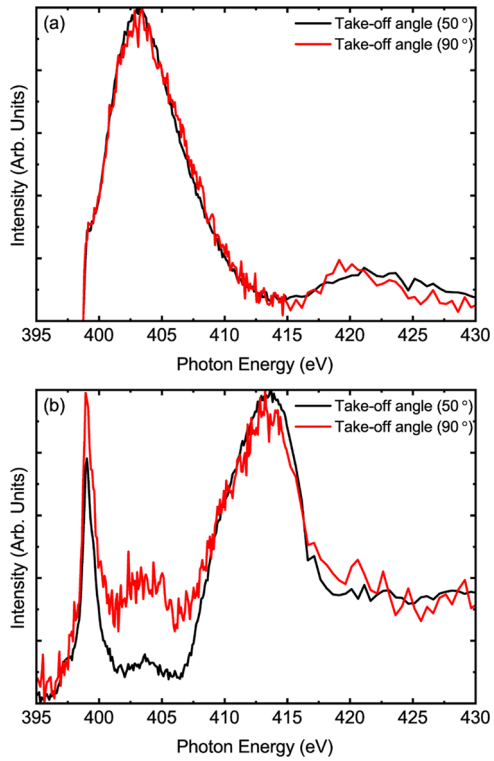

Figure 5. (a) SiNx and (b) N−C species for N K-edge XANES spectra each measured at two different takeoff angles of 90° (surface normal) and 50°.

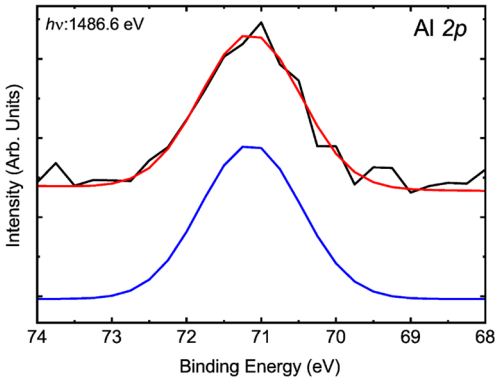

Figure 6. Al 2p core-level XPS spectroscopy for Al-doped 4H-SiC(0001).

edge peak appears at 1556 eV, and it is attributed to the 1s→ p transitions, where p states are hybridized with Al 3s states.[55,56] The peak at 1565 eV is due to the Al 1s→ Al 3p transition,[55,57] while the peak at 1579 eV is attributed to the multiple scattering from several atomic shells.[55,58,59]

In order to clarify the atomic structure of the active dopant site for Al-doped 4H-SiC(0001), we performed XANES simulations. Based on a previous study, Si substitutional (Al_{Si}) and C substitutional (Al_c) sites were proposed as the Al dopant structures in 4H-SiC, which is shown in Figure 7 (b) and 7(c), respectively.[60] Therefore, for the simulations with Al-doped 4H-SiC(0001), we used cluster sizes of ∼350 and ∼200 atoms for Al_{Si} and Al_c, respectively.

For the simulated Al_{Si} spectrum, the simulated absorption edge was observed at an energy different from that of the experimental one. Thus, the absorption edge was shifted by 6.5

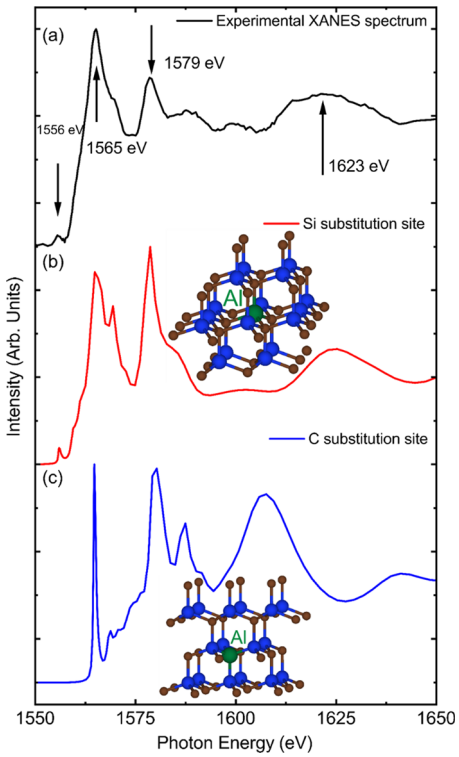

Figure 7. (a) Al *K*-edge XANES spectrum for Al-doped 4H-SiC(0001). The simulated XANES spectra of (b) Al_{Si} (red line) and (c) Al_C (blue line). In the FEFF9 simulations, the many-body amplitude reduction factor was set to 1.0. The cluster sizes of the Sub states are 9.5 Å (Si) and 8 Å (C), which include ∼350 and ∼200 atoms, respectively. The final state effect (Z+1 approximation) was employed. The inset shows each local atomic structure of Al_{Si} and Al_C in 4H-SiC. Dark blue, brown, and green circles indicate Si, C, and Al, respectively.

eV to eliminate the calculation error in the present simulations. These energy shifts are commonly observed from 3 eV to more than 10 eV in the simulated XANES spectra based on FEFF9.[19,20,61−63]

For the Al_{Si} simulated XANES spectrum, peaks are observed at 1565, 1569, 1579, and 1623 eV. The peak at 1565 eV is due to the Al 1s→ Al 3p transition,[55,57] while the peaks at 1569 and 1579 eV are attributed to the multiple scattering from several atomic shells.[55,58,59] These energy peak positions and the spectrum features are in good agreement with those of the experimental XANES spectrum. According to a previous study based on DFT calculation, Al_{Si} exhibits the lower formation energy than Al_C.[64] Thus, Al_{Si} is the atomic structure of the active dopant site for Al-doped 4H-SiC(0001).

To further investigate changes in the interatomic bond length around the dopant Al atom and in the coordination numbers of the dopant Al atom for Al-doped 4H-SiC(0001), we employed EXAFS measurements. Figure 8(a) and 8(b) shows the EXAFS spectrum and oscillations for Al-doped 4H-SiC(0001), respectively. Because the Si K-edge appears at 300 eV higher energy than the Al *K*-edge, the energy range of EXAFS measurements is limited. Therefore, the range in k-space was chosen at 2−5.9 $Å^{-1}$ with a good signal-to-noise ratio.

Figure 8(c) shows the Fourier transforms of the k^3-weighted EXAFS spectrum (Figure 8(b)). The fitting was performed using ARTEMIS software, where the reliable factor (r factor)

https://doi.org/10.1021/acsaelm.3c00546
ACS Appl. Electron. Mater. 2023, 5, 3843−3850

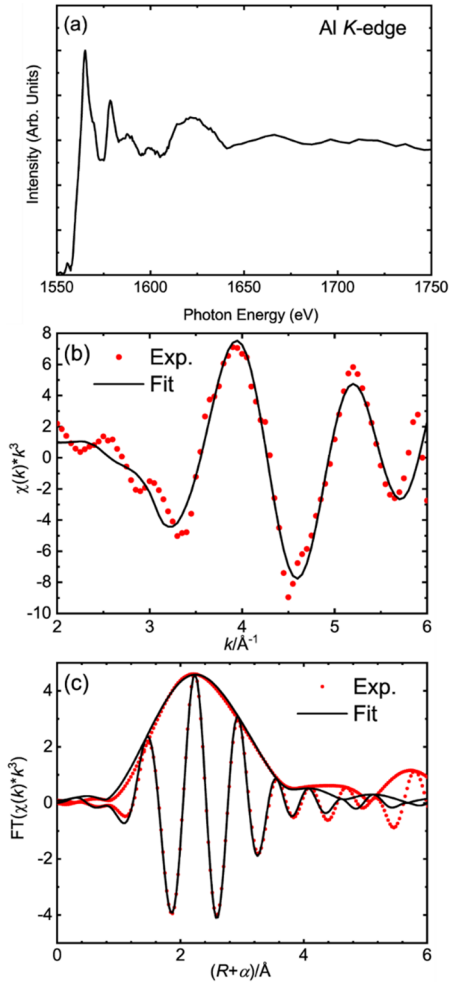

Figure 8. (a) Al *K*-edge EXAFS spectrum and (b) k^3-weighted Al *K*-edge EXAFS spectrum (red dots) plotted with best fits (black) for Al-doped 4H-SiC sample. (c) Fourier transforms of the k^3-weighted EXAFS spectrum (red dots) plotted with fits (black) for Al-doped 4H-SiC. The fitting range is 1−4 Å for the first nearest-neighbor distance with amplitude reduction factors, Δ*R*, and MSRD values set to 0.8, 0.238, and 0.002 (without phase shift correction).

was set to 0.0032 under k^3 weights in the 2−5.9 $Å^{-1}$ k range. We used the paths of 4H-SiC. The fitting range was chosen at 1−4 Å in *r* space. From the fitting, the coordination number and the Al−C distance were estimated to be 4.0 and 2.13 Å, respectively. Since the undoped SiC exhibits a coordination number of 4.0 and a Si−C bond length of 1.89 Å, the Al dopant atom increases the bond length around the dopant.[65,66] This may be due to the difference in atom size between the Al atom (radius: 0.125 nm) and the Si atom (radius: 0.111 nm).[67] The derivation of the bond length may be attributed to the relaxation of the local structure around the dopant Al atom.

It is worth noting that XANES simulations with the bond length of Al−C are 2.13 Å in Al-doped 4H-SiC. For the above XANES simulations in Figure 7, we ignored an increase in Al−C bond length. We performed XANES simulations in which increase in Al−C bond length is included, and then we found that the XANES simulations with increase in Al−C bond length shows much better than nonexpansion simulation result (Figure 7) (See Figure S6).

4. CONCLUSION

Using XANES, EXAFS, AES, and PES, we investigated the atomic structures and chemical states of the active and inactive dopant atoms in N- and Al-doped 4H-SiC(0001). In the case of N-doped 4H-SiC(0001), PES showed that there were two chemical states. We fitted the AES spectrum using the Voigt function though Auger electron emitted processes are very complicated. Both experimental and simulated XANES showed that the active dopant site is N_C, whereas the inactive dopant state was due to the N−C species.

In the case of Al-doped 4H-SiC(0001), the dopant Al atom had one chemical state. From XANES, the active dopant state is Al_{Si}. EXAFS showed that the bond length between the Al and C atoms increased compared to the case of undoped 4H-SiC. In Al-doped 4H-SiC(0001), the relaxation of the local structure may occur because the dopant Al atom increases the bond length due to the difference in atomic size between the Al and the Si atoms.

■ ASSOCIATED CONTENT

Supporting Information

The Supporting Information is available free of charge at https://pubs.acs.org/doi/10.1021/acsaelm.3c00546.

Extensive experimental data. Figure S1 shows XPS spectra of N-doped 4H-SiC(0001). Figure S2 shows XPS and HAXPES spectra of Al-doped 4H-SiC(0001). Figure S3 shows cluster size and parameters for FEFF9 calculations of N-doped 4H-SiC. Figure S4 shows FEFF9 calculations of N-doped 4H-SiC for interstitial sites and carbon vacancies. Figure S5 shows cluster size and parameters for FEFF9 calculations of Al-doped 4H-SiC. Figure S6 shows XANES simulation spectrum in Al-doped 4H-SiC for Al−C bond expansion comparison (PDF)

■ AUTHOR INFORMATION

Corresponding Author

Yoshiyuki Yamashita − *National Institute for Materials Science (NIMS), Tsukuba 305-0044 Ibaraki, Japan; Department of Applied Chemistry, Faculty of Engineering, Kyushu University, Fukuoka 819-0395, Japan;* orcid.org/0000-0003-0994-8095; Email: YAMASHITA.Yoshiyuki@nims.go.jp

Authors

Yuhua Tsai − *National Institute for Materials Science (NIMS), Tsukuba 305-0044 Ibaraki, Japan; Department of Applied Chemistry, Faculty of Engineering, Kyushu University, Fukuoka 819-0395, Japan;* orcid.org/0000-0001-7996-6681

Jingmin Tang − *National Institute for Materials Science (NIMS), Tsukuba 305-0044 Ibaraki, Japan; Department of Applied Chemistry, Faculty of Engineering, Kyushu University, Fukuoka 819-0395, Japan*

Complete contact information is available at: https://pubs.acs.org/10.1021/acsaelm.3c00546

Notes

The authors declare no competing financial interest.

https://doi.org/10.1021/acsaelm.3c00546
ACS Appl. Electron. Mater. 2023, 5, 3843−3850

■ ACKNOWLEDGMENTS

We acknowledge Dr. M. Nakatake and Dr. H. Sugiyama at the Aichi Synchrotron Center for the experimental support.

■ REFERENCES

(1) Xu, Q.; Sun, H. Y.; Chen, C.; Jang, L. Y.; Rusli, E.; Mendis, S. P.; Tin, C. C.; Qiu, Z. R.; Wu, Z. Y.; Liu, C. W.; Feng, Z. C. 4H-SiC Wafers Studied by X-Ray Absorption and Raman Scattering. *Mater. Sci. Forum* **2012**, *717*−*720*, 509−512.

(2) Roccaforte, F.; Fiorenza, P.; Vivona, M.; Greco, G.; Giannazzo, F. Selective Doping in Silicon Carbide Power Devices. *Materials* **2021**, *14*, 3923.

(3) Liu, G.; Tuttle, B. R.; Dhar, S. Silicon Carbide: A Unique Platform for Metal-Oxide-Semiconductor Physics. *Applied Physics Reviews* **2015**, *2*, No. 021307.

(4) Usman, M.; Arshad, M.; Suvanam, S. S.; Hallén, A. Influence of Annealing Environment on the ALD-Al_2O_3/4h-SiC Interface Studied through XPS. *J. Phys. D: Appl. Phys.* **2018**, *51*, 105111.

(5) Paneerselvam, E.; Lakshmi Narayanan, V. K.; Vasa, N. J.; Higashihata, M.; Nakamura, D.; Ikenoue, H.; Ramachandra Rao, M. S. Laser Assisted Doping of Silicon Carbide Thin Films Grown by Pulsed Laser Deposition. *J. Electron. Mater.* **2019**, *48*, 3468−3478.

(6) Isomura, N.; Nonaka, T.; Watanabe, Y. Local Atomic Structure Analysis of SiO_2/SiC Interfaces Using X-ray Absorption Spectroscopy. *R&D Review of Toyota CRDL* **2019**, *50*, 11−17.

(7) Fiorenza, P.; Giannazzo, F.; Roccaforte, F. Characterization of SiO_2/4H-SiC Interfaces in 4H-SiC MOSFETs: A Review. *Energies* **2019**, *12*, 2310.

(8) Ohkubo, M.; Shiki, S.; Ukibe, M.; Matsubayashi, N.; Kitajima, Y.; Nagamachi, S. X-Ray Absorption near Edge Spectroscopy with a Superconducting Detector for Nitrogen Dopants in SiC. *Sci. Rep.* **2012**, *2*, 1−5.

(9) Laube, M.; Schmid, F.; Pensl, G.; Wagner, G.; Linnarsson, M.; Maier, M. Electrical Activation of High Concentrations of N^+ and P^+ Ions Implanted into 4H−SiC. *J. Appl. Phys.* **2002**, *92*, 549−554.

(10) Ji, S. Y.; Kojima, K.; Ishida, Y.; Tsuchida, H.; Yoshida, S.; Okumura, H. Low Resistivity, Thick Heavily Al-Doped 4h-SiC Epilayers Grown by Hot-Wall Chemical Vapor Deposition. *Mater. Sci. Forum* **2013**, *740*, 181−184.

(11) Huh, S. W.; Chung, H. J.; Benamara, M.; Skowronski, M.; Sumakeris, J. J.; Paisley, M. J. Doping-Induced Strain and Relaxation of Al-Doped 4h-SiC Homoepitaxial Layers. *J. Appl. Phys.* **2004**, *96*, 4637−4641.

(12) Beltrán, A. M.; Duguay, S.; Strenger, C.; Bauer, A. J.; Cristiano, F.; Schamm-Chardon, S. Atomic Scale Characterization of SiO_2/4H-SiC Interfaces in MOSFETs Devices. *Solid State Commun.* **2015**, *221*, 28−32.

(13) Zhang, L.; Diallo, L.; Fnidiki, A.; Lechevallier, L.; Declémy, A.; Lefebvre, W.; Juraszek, J. Probing the Origins of Magnetism in 2 At% Fe-implanted 4H-SiC. *Scripta Materialia* **2020**, *188*, 157−163.

(14) Yamashita, S.; Kikkawa, J.; Yanagisawa, K.; Nagai, T.; Ishizuka, K.; Kimoto, K. Atomic Number Dependence of *Z* Contrast in Scanning Transmission Electron Microscopy. *Sci. Rep.* **2018**, *8*, 1−11.

(15) Shekhawat, R. S.; Singh, N. J.; Shakil, M.; Kumar, P.; Kumar, D.; Kumar, P.; Singh, A. K.; Kothari, P.; Das, S.; Prajapat, P.; Panwar, D. K.; Kumar, S.; Eshwar, T.; Singh, S.; Singh, D. Optimization of Thermal Oxidation for 4H-SiC and Fabricate/Characterize MOS Capacitor. *IOP Conference Series: Materials Science and Engineering* **2021**, *1119*, No. 012014.

(16) Isomura, N.; Kamada, M.; Nonaka, T.; Nakamura, E.; Takano, T.; Sugiyama, H.; Kimoto, Y. A New EXAFS Method for the Local Structure Analysis of Low-Z Elements. *Journal of Synchrotron Radiation* **2016**, *23*, 281−285.

(17) Tang, J.; Yamashita, Y. Atomic Structures and Chemical States of Active and Inactive Dopant Sites in Si-Doped GaN. *ACS Applied Electronic Materials* **2021**, *3*, 4618−4622.

(18) Wang, S.; An, Y.; Li, X.; Wu, Z.; Liu, J. Effect of Mn Doping on the Structural, Magnetic and Transport Properties of SIC Films. *J. Alloys Compd.* **2014**, *584*, 339−343.

(19) Nakanishi, K.; Ohta, T. Verification of the FEFF Simulations to K-Edge XANES Spectra of the Third Row Elements. *J. Phys.: Condens. Matter* **2009**, *21*, 104214.

(20) Rehr, J. J.; Kas, J. J.; Vila, F. D.; Prange, M. P.; Jorissen, K. Parameter-Free Calculations of X-Ray Spectra with FEFF9. *Phys. Chem. Chem. Phys.* **2010**, *12*, 5503−5513.

(21) Rehr, J. J.; Kas, J. J.; Prange, M. P.; Sorini, A. P.; Takimoto, Y.; Vila, F. Ab Initio Theory and Calculations of X-Ray Spectra. *Comptes Rendus Physique* **2009**, *10*, 548−559.

(22) Rehr, J. J.; Albers, R. C. Theoretical Approaches to X-Ray Absorption Fine Structure. *Rev. Mod. Phys.* **2000**, *72*, 621−654.

(23) Alperovich, I.; Moonshiram, D.; Soldatov, A.; Pushkar, Y. Ru $L_{2,3}$ XANES Theoretical Simulation with DFT: A Test of the Core-Hole Treatment. *Solid State Commun.* **2012**, *152*, 1880−1884.

(24) Roy, M.; Gurman, S. J. An Investigation of the Use of the Hedin−Lundqvist Exchange and Correlation Potential in EXAFS Data Analysis. *Journal of Synchrotron Radiation* **2001**, *8*, 1095−1102.

(25) Hamada, K.; Mikami, A.; Naruoka, H.; Yamabe, K. Analysis of Nitrogen State on MOS Interface of 4H-SiC M-Face after Nitric Oxide Post Oxidation Annealing (NO-POA). *e-Journal of Surface Science and Nanotechnology* **2017**, *15*, 109−114.

(26) Chourasia, A. R.; Hood, S. J.; Chopra, D. R. A Study of SI Compounds by Zr *Lα* Photoelectron Spectroscopy. *Journal of Vacuum Science & Technology A: Vacuum, Surfaces, and Films* **1996**, *14*, 699−703.

(27) Batan, A.; Franquet, A.; Vereecken, J.; Reniers, F. Characterisation of the Silicon Nitride Thin Films Deposited by Plasma Magnetron. *Surf. Interface Anal.* **2008**, *40*, 754−757.

(28) Matsuoka, M.; Isotani, S.; Sucasaire, W.; Zambom, L. S.; Ogata, K. Chemical Bonding and Composition of Silicon Nitride Films Prepared by Inductively Coupled Plasma Chemical Vapor Deposition. *Surf. Coat. Technol.* **2010**, *204*, 2923−2927.

(29) Dementjev, A. P.; de Graaf, A.; van de Sanden, M. C. M.; Maslakov, K. I.; Naumkin, A. V.; Serov, A. A. X-Ray Photoelectron Spectroscopy Reference Data for Identification of the C_3N_4 Phase in Carbon−Nitrogen Films. *Diamond Relat. Mater.* **2000**, *9*, 1904−1907.

(30) Yan, H.; Chen, Y.; Xu, S. Synthesis of Graphitic Carbon Nitride by Directly Heating Sulfuric Acid Treated Melamine for Enhanced Photocatalytic H_2 Production from Water under Visible Light. *Int. J. Hydrogen Energy* **2012**, *37*, 125−133.

(31) Fernandes, R. A.; Sampaio, M. J.; Da Silva, E. S.; Boumeriame, H.; Lopes, T.; Andrade, L.; Mendes, A.; Faria, J. L.; Silva, C. G. Sustainable Production of Value-Added Chemicals and Fuels by Using a Citric Acid-Modified Carbon Nitride Optical Semiconductor. *Applied Catalysis A: General* **2021**, *609*, 117912.

(32) Maddi, C.; Bourquard, F.; Barnier, V.; Avila, J.; Asensio, M.-C.; Tite, T.; Donnet, C.; Garrelie, F. Nano-Architecture of Nitrogen-Doped Graphene Films Synthesized from a Solid CN Source. *Sci. Rep.* **2018**, *8*, 1−13.

(33) Jiang, H.; Liu, L.; Zhao, K.; Liu, Z.; Zhang, X.; Hu, S. Effect of Pyridinic- and Pyrrolic-Nitrogen on Electrochemical Performance of Pd for Formic Acid Electrooxidation. *Electrochim. Acta* **2020**, *337*, 135758.

(34) Seah, M. P.; Dench, W. A. Quantitative Electron Spectroscopy of Surfaces: A Standard Data Base for Electron Inelastic Mean Free Paths in Solids. *Surf. Interface Anal.* **1979**, *1*, 2−11.

(35) Chourasia, A. R.; Chopra, D. R. A Study of SI_3N_4 by XPS. *Surface Science Spectra* **1993**, *2*, 117−122.

(36) Boyd, K. J.; Marton, D.; Todorov, S. S.; Al-Bayati, A. H.; Kulik, J.; Zuhr, R. A.; Rabalais, J. W. Formation of C−N Thin Films by Ion Beam Deposition. *Journal of Vacuum Science & Technology A: Vacuum, Surfaces, and Films* **1995**, *13*, 2110−2122.

(37) Ripalda, J. M.; García de Abajo, F. J.; Montero, I.; Galán, L.; Van Hove, M. A. Photoelectron Diffraction at the Surface of Amorphous Carbon Nitride. *Appl. Phys. Lett.* **2000**, *77*, 3394−3396.

https://doi.org/10.1021/acsaelm.3c00546
ACS Appl. Electron. Mater. 2023, 5, 3843−3850

(38) Madden, H. H.; Holloway, P. H. AES Investigation of the Chemical Structure of Silicon Oxy-Nitride Films. *J. Vac. Sci. Technol.* **1979**, *16*, 618−621.
(39) Tanuma, S.; Powell, C. J.; Penn, D. R. Calculations of Electron Inelastic Mean Free Paths (IMFPS). Iv. Evaluation of Calculated Imfps and of the Predictive IMFP Formula TPP-2 for Electron Energies between 50 and 2000 EV. *Surf. Interface Anal.* **1993**, *20*, 77−89.
(40) Tanuma, S.; Powell, C. J.; Penn, D. R. Calculations of Electron Inelastic Mean Free Paths. Ix. Data for 41 Elemental Solids over the 50 EV to 30 Kev Range. *Surf. Interface Anal.* **2011**, *43*, 689−713.
(41) Yabuta, H.; Uesugi, M.; Naraoka, H.; Ito, M.; Kilcoyne, A. L. D.; Sandford, S. A.; Kitajima, F.; Mita, H.; Takano, Y.; Yada, T.; Karouji, Y.; Ishibashi, Y.; Okada, T.; Abe, M. X-Ray Absorption near Edge Structure Spectroscopic Study of Hayabusa Category 3 Carbonaceous Particles. *Earth, Planets and Space* **2014**, *66*, 1−8.
(42) Latham, K. G.; Simone, M. I.; Dose, W. M.; Allen, J. A.; Donne, S. W. Synchrotron Based NEXAFS Study on Nitrogen Doped Hydrothermal Carbon: Insights into Surface Functionalities and Formation Mechanisms. *Carbon* **2017**, *114*, 566−578.
(43) Franke, R.; Bender, S.; Pavlychev, A. A.; Kroll, P.; Riedel, R.; Greiner, A. Si and N K-XANES Spectroscopic Study of Novel Si−C−N Ceramics. *J. Electron Spectrosc. Relat. Phenom.* **1998**, *96*, 253−257.
(44) Jiménez, I.; Tong, W. M.; Shuh, D. K.; Holloway, B. C.; Kelly, M. A.; Pianetta, P.; Terminello, L. J.; Himpsel, F. J. Bonding Modifications in Carbon Nitride Films Induced by Thermal Annealing: An X-Ray Absorption near Edge Study. *Appl. Phys. Lett.* **1999**, *74*, 2620−2622.
(45) Bhattacharyya, S.; Lübbe, M.; Richter, F. Near Edge X-Ray Absorption Fine Structure of Thermally Annealed Amorphous Nitrogenated Carbon Films. *J. Appl. Phys.* **2000**, *88*, 5043−5049.
(46) Horsley, J. A.; Stöhr, J.; Hitchcock, A. P.; Newbury, D. C.; Johnson, A. L.; Sette, F. Resonances in the *k* Shell Excitation Spectra of Benzene and Pyridine: Gas Phase, Solid, and Chemisorbed States. *J. Chem. Phys.* **1985**, *83*, 6099−6107.
(47) Hövel, S.; Kolczewski, C.; Wühn, M.; Albers, J.; Weiss, K.; Staemmler, V.; Wöll, C. Pyridine Adsorption on the Polar ZnO(0001) Surface: Zn Termination versus O Termination. *J. Chem. Phys.* **2000**, *112*, 3909−3916.
(48) Lee, J. H.; Ryu, J.; Kim, J. Y.; Nam, S.-W.; Han, J. H.; Lim, T.-H.; Gautam, S.; Chae, K. H.; Yoon, C. W. Carbon Dioxide Mediated, Reversible Chemical Hydrogen Storage Using a PD Nanocatalyst Supported on Mesoporous Graphitic Carbon Nitride. *Journal of Materials Chemistry A* **2014**, *2*, 9490−9495.
(49) Apen, E.; Hitchcock, A. P.; Gland, J. L. Experimental Studies of the Core Excitation of Imidazole, 4,5-Dicyanoimidazole, and S-Triazine. *J. Phys. Chem.* **1993**, *97*, 6859−6866.
(50) Chuang, C.-H.; Ray, S. C.; Mazumder, D.; Sharma, S.; Ganguly, A.; Papakonstantinou, P.; Chiou, J.-W.; Tsai, H.-M.; Shiu, H.-W.; Chen, C.-H.; Lin, H.-J.; Guo, J.; Pong, W.-F. Chemical Modification of Graphene Oxide by Nitrogenation: An X-Ray Absorption and Emission Spectroscopy Study. *Sci. Rep.* **2017**, *7*, 42235.
(51) Ferro, G.; Chaussende, D. A New Model for in Situ Nitrogen Incorporation into 4H-SiC during Epitaxy. *Sci. Rep.* **2017**, *7*, 43069.
(52) Khatami, Z.; Bleczewski, L.; Neville, J. J.; Mascher, P. X-Ray Absorption Spectroscopy of Silicon Carbide Thin Films Improved by Nitrogen for All-Silicon Solar Cells. *ECS Journal of Solid State Science and Technology* **2020**, *9*, No. 083002.
(53) Lin, L.; Liu, T.; Zhang, Z.; Tao, H.; He, M.; Song, B.; Zhang, Z. Vacancy Induced Magnetism in N-Doped 4H−SiC by First-Principle Calculations. *Solid State Sci.* **2015**, *49*, 78−82.
(54) Tang, J.; Takeuchi, S.; Tanaka, M.; Tomita, H.; Hashimoto, Y.; Nagata, T.; Chen, J.; Ohkochi, T.; Kotani, Y.; Matsushita, T.; Yamashita, Y. Direct Observation of Atomic Structures and Chemical States of Active and Inactive Dopant Sites in Mg-Doped Gan. *ACS Applied Electronic Materials* **2022**, *4*, 4719−4723.
(55) Li, D.; Bancroft, G. M.; Fleet, M. E.; Feng, X. H.; Pan, Y. Al K-Edge XANES Spectra of Aluminosilicate Minerals. *Am. Mineral.* **1995**, *80*, 432−440.
(56) Cabaret, D.; Brouder, C. Origin of the Pre-Edge Structure at the Al *k*-Edge: The Role of Atomic Vibrations. *Journal of Physics: Conference Series* **2009**, *190*, No. 012003.
(57) Wong, J.; Tanaka, T.; Rowen, M.; Schäfers, F.; Müller, B. R.; Rek, Z. U. Yb_{66}− A New Soft X-Ray Monochromator for Synchrotron Radiation. *II. Characterization. Journal of Synchrotron Radiation* **1999**, *6*, 1086−1095.
(58) Ildefonse, P.; Cabaret, D.; Sainctavit, P.; Calas, G.; Flank, A.-M.; Lagarde, P. Aluminium X-Ray Absorption near Edge Structure in Model Compounds and Earth's Surface Minerals. *Physics and Chemistry of Minerals* **1998**, *25*, 112−121.
(59) Prado, R. J.; Fantini, M. C.; Carreño, M. N.; Pereyra, I.; Flank, A. M. Al Thermal Diffusion in *a*-$Si_{1-x}C_x$:H Thin Film Studied by XAFS. *AIP Conf. Proc.* **2007**, *882* (1), 529−531.
(60) Miyata, M.; Higashiguchi, Y.; Hayafuji, Y. *Ab Initio* Study of Substitutional Impurity Atoms in 4H-SiC. *J. Appl. Phys.* **2008**, *104*, 123702.
(61) Bosman, E.; Thieme, J. Modeling of Xanes-Spectra with the FEFF-Program. *Journal of Physics: Conference Series* **2009**, *186*, No. 012004.
(62) Balde, C. P. Sodium Alanate nanoparticles for hydrogen storage, PhD Thesis, Utrecht University: Utrecht, The Netherlands, 2008.
(63) Mathew, K.; Zheng, C.; Winston, D.; Chen, C.; Dozier, A.; Rehr, J. J.; Ong, S. P.; Persson, K. A. High-Throughput Computational X-Ray Absorption Spectroscopy. *Sci. Data* **2018**, *5*, 1−8.
(64) Lu, L.; Zhang, H.; Wu, X.; Shi, J.; Sun, Y.-Y. Atomic and Electronic Structures of P-Type Dopants in 4H-SiC. *Chinese Physics B* **2021**, *30*, No. 096806.
(65) Zeng, W.; Feng, Z. C.; Zheng, R. S.; Jang, L. Y.; Liu, C. W. 3c-, 4H- And 6H-SiC Bulks Studied by Silicon *k*-Edge X-Ray Absorption. *Mater. Sci. Forum* **2013**, *740*, 573−576.
(66) Isomura, N.; Kosaka, S.; Kataoka, K.; Watanabe, Y.; Kimoto, Y. X-Ray Absorption Spectroscopy Study on SiC-Side Interface Structure of SiO_2−SiC Formed by Thermal Oxidation in Dry Oxygen. *Jpn. J. Appl. Phys.* **2018**, *57*, No. 060308.
(67) Slater, J. C. Atomic Radii in Crystals. *J. Chem. Phys.* **1964**, *41*, 3199−3204.

https://doi.org/10.1021/acsaelm.3c00546
ACS Appl. Electron. Mater. 2023, 5, 3843−3850